JOURNAL OF PROPULSION AND POWER
Vol. 25, No. 6, November–December 2009

Computational Simulation of Cylindrical Film Hole with Jet Pulsation on Flat Plates

Olga Kartuzova,* Daniel Danila,* and Mounir B. Ibrahim†
Cleveland State University, Cleveland, Ohio 44115-2425
and
Ralph J. Volino‡
U.S. Naval Academy, Annapolis, Maryland 21402

DOI: 10.2514/1.40299

Film cooling of flat plates with pulsation were simulated using FLUENT™ commercial code with realizable *k-ε* turbulence model. The simulations were done for nominal blowing ratios 0.5 and 1.5, duty cycle = 50%, and Strouhal number ranging from 0.0119 to 1.0. Pulsation helps to lower the amount of cool air from the compressor, which is desirable for film-cooling applications. Pulsed jets performance significantly depends on geometry and blowing ratio. From the cases studied and for steady flow with attached jets, pulsation considerably decreases the film-cooling effectiveness. On the other hand, for steady flow cases where jet liftoff occurs (e.g., higher blowing ratios), pulsation helps to increase the film-cooling effectiveness.

Nomenclature

B	=	blowing ratio $= \rho_c V_c / \rho_\infty V_\infty$
D	=	film hole diameter, m
f	=	frequency, Hz
L	=	Length of film-cooling hole channel, m
Re	=	Reynolds number $= V_\infty D/\nu$
St	=	Strouhal number $= fD/V_\infty$
T	=	local fluid temperature, K
t	=	time/(cycle time)
V	=	local fluid velocity magnitude, m/s
x	=	streamwise distance along the test plate, m
y	=	vertical distance above the test plate, m
y^+	=	dimensionless wall distance $= y(\tau_w/\rho_w)^{1/2}/V_w$
z	=	spanwise coordinate, distance from centerline of the hole, m
η	=	adiabatic film cooling effectiveness $=(T_{\text{aw}} - T_\infty)/(T_{\text{jet}} - T_\infty)$
θ	=	dimensionless temperature, $(T - T_\infty)/(T_{\text{jet}} - T_\infty)$
ν	=	kinematic viscosity, m^2/s
ρ	=	density, kg/m^3

Subscripts

aw	=	adiabatic wall
c	=	coolant flow characteristics
fh	=	film hole
jet	=	film-cooling jet characteristics
∞	=	mainstream

I. Introduction

FILM cooling has been used in modern gas turbines to protect the surface of turbine blades from failing at high temperatures. Much research has been done in film cooling to achieve better cooling of gas turbine blades and thus increase performance of turbine engines by allowing higher inlet temperatures. About 20–25% of compressor air is used for cooling high-performance turbine engines (Ekkad et al. [1]). Higher engine efficiency may be obtained by minimizing coolant mass flow with the same or higher film-cooling effectiveness. Experimental studies found in the literature showed that coolant flow pulsation might help to improve film cooling while reducing the actual film flow rate. There are very few studies published that consider the effect of jet pulsation on the film-cooling characteristics.

Ekkad et al. [1] experimentally investigated the effect of jet pulsation and duty cycle on film cooling from a single jet located on the circular leading edge of a blunt body. Film-cooling characteristics were examined for duty cycles (DC) (from 0.1 to 1) at nominal pulse blowing ratios (B) (from 0.5 to 2) and pulse frequencies of 5 and 10 Hz. This study reported that higher film-cooling effectiveness was obtained at the reduced blowing ratios, and the effect of varying the pulsing frequency was negligible. The conclusion of this work was that pulsed jets resulted in relatively better film-cooling effectiveness compared to continuously blown jets.

Coulthard et al. [2] conducted an experimental study of a row of film-cooling jets in crossflow on a flat plate. Jets were inclined 35 deg to the surface in a streamwise direction. Various blowing ratios (from 0.25 to 1.5), duty cycles (from 0.25 to 0.75), and Strouhal numbers St (from 0.0119 to 0.1905) were considered. The authors reported that the highest film-cooling effectiveness was achieved at blowing ratio 0.5 with steady blowing. With increasing blowing ratio, effectiveness decreased due to jet liftoff. In their work the authors observed that higher pulsation frequencies resulted in lower effectiveness with the exception of the highest frequency tested, where the trend was reversed. The overall conclusion was that pulsing does not provide benefits to the film-cooling applications for the studied geometry and flow characteristics. Comparing the results of the two experiments (Ekkad et al. [1] and Coulthard et al. [2]) is rather difficult because the two cases had different geometry (both jet and plenum) and free-stream pressure gradients, in addition to other differences.

Muldoon and Acharya [3] were the first to conduct a computational direct numerical simulation (DNS) study of pulsed jet film cooling. The geometry in their work consisted of a cylindrical jet, inclined at 35 deg in the streamwise direction, in a crossflow. Jets were pulsed with various duty cycles (from 0.25 to 1), blowing ratios (from 0.375 to 1.5), and Strouhal numbers (0.08 and 0.32). The coolant delivery tube was modeled in baseline DNS calculations to obtain jet-exit conditions. A conclusion of their study was that pulsing, with higher frequency DC = 50% and peak B of 1.5, helped

Received 6 August 2008; accepted for publication 11 May 2009.

*Graduate Student, Mechanical Engineering Department.
†Professor, Mechanical Engineering Department; m.ibrahim@csuohio.edu. Associate Fellow AIAA.
‡Professor, Department of Mechanical Engineering; volino@usna.edu.

Table 1 Pulsed jet cases simulated in the present study

Geometry	CFH	
Blowing ratio	$B = 0.5$	$B = 1.5$
Turbulence model	SKE, SKW, RKE, V2F	RKE
Strouhal number	Steady state, $St = 0.0119$, 0.19, 0.38, and 1	
Density ratio	1.0	

to improve film-cooling effectiveness (due to reduced jet liftoff) compared to the steady $B = 1.5$ case.

Results on pulsed jets' effects on film cooling found in the literature are mixed. Comprehensive pulsed jets film-cooling studies are needed to answer the question of when and where jets' pulsation can help to improve film cooling, while reducing the coolant flow rate.

The purpose of the present work is to investigate pulse frequency and blowing ratio effects on film cooling to identify under which conditions jet pulsation has better performance and explain the flow physics behind it.

FLUENT^{TM} [4] commercial code with a realizable k-ε turbulence model was used in this study to investigate how the pulsed jet performance was affected by varying pulsation frequency and blowing ratio.

II. Numerical Simulation Details

Ten different cases were simulated in the present study for CFH (Cylindrical Film Hole) geometry of Coulthard et al. [2]. Details of all cases are presented in Table 1.

A. Modeling and Boundary Conditions

The CFH geometry matched the experiment of Coulthard et al. [2]. The schematic of the experimental test setup is presented in Fig. 1. The extent of the computational domain used in the present work is shown by the dashed lines. It is 0.8 D upstream, 18 D downstream of the jet leading edge (LE) and 5.25 D above the test surface. Jets are inclined at a 35 deg angle in a streamwise direction and spaced 3 D apart center-to- center. Film hole length to diameter ratio $L/D = 4$. The origin of the Cartesian coordinate system is placed at the trailing edge (TE) of the film hole on the top surface of the test plate and its x, y, and z axes aligned with the streamwise, vertical, and lateral direction. Computational domain includes the whole supply plenum because the flow in the film hole is complex and highly depends on the plenum geometry (Walters and Leylek [5,6]). Incompressible fluid flow was considered.

GAMBIT 2.3.16 software by Fluent, Inc. was used to generate highly refined grid, consisting of about two million cells. Highly refined grid near the wall resulted in average $y^+ \approx 0.75$ for the injection pipe walls and $y^+ \approx 0.65$ for the cooled plate.

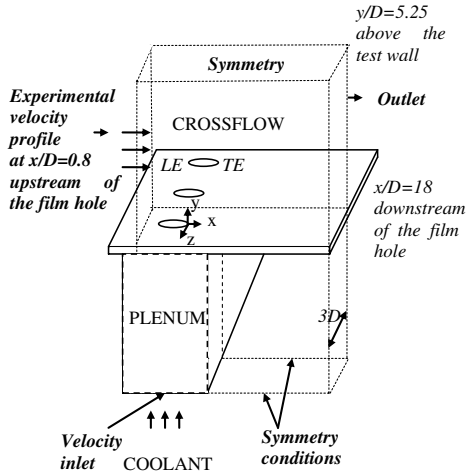

Fig. 1 A schematic of the experimental test setup for Coulthard et al. [2] CFH geometry, including extent of the computational domain (dashed lines) and boundary conditions.

The experimental velocity profile of Coulthard et al. [2] was applied at $x/D = 0.8$ upstream of the film hole LE in combination with the profiles for TKE (turbulent kinetic energy) and the turbulence dissipation rate. It represented fully turbulent boundary layers at this location. Symmetry boundary conditions were modeled at $z/D = 1.5$ and -1.5 from the jet centerline. Symmetry rather than periodic boundary conditions were justified on the grounds of: 1) the results from Coulthard et al. [2] showed symmetry and 2) most of the computational fluid dynamics (CFD) data were presented for time-averaged quantities where the differences between the two boundary conditions (symmetry and periodic) are negligible. Symmetry was also applied at the top of the computational domain. Temperature of the crossflow air was set to 293 K. Crossflow inlet parameters were maintained the same for all cases. Inlet plenum geometry of Coulthard et al. [2] was used with coolant injection through round holes (diameter (D) = 0.019 m) at the bottom of the plenum. The plenum inlet velocity was modified to change the blowing ratio. The coolant temperature of 300 K corresponds to a density ratio near 1. Reynolds number, based on freestream velocity and film hole diameter, is 10,400. All the walls were defined as no-slip and adiabatic. In pulsed cases the blowing ratio was calculated as an average blowing ratio during the open-jet period. At the outlet a constant pressure boundary condition was applied with zero gauge pressure.

The choice of turbulence model for this geometry will be discussed later in the Code Validation section. Computations were performed using version 6.3.26 of the finite-volume code FLUENT^{TM}.

B. Convergence

Because of high flow unsteadiness, even for steady blowing, unsteady calculations were performed for pulsed and unpulsed cases. Convergence was established when 1) residuals reduced to a value 10^{-5} except energy residual for which convergence criterion was 10^{-8}, 2) no change was observed in any field results for steady cases and cycle-to-cycle convergence was achieved for pulsed cases, and 3) the mass and energy imbalance was less than 0.01%.

Approximately 800 time steps with time step size = 0.01 s were necessary to reach a fully converged state for steady blowing cases. For the pulsed cases 10–15 cycles were needed to achieve cycle-to-cycle convergence with 20 time steps per cycle, and 20–50 iterations per time step. Time step size was adjusted with the pulse frequency such that the same number of time steps per cycle was used for all cases.

III. Turbulence Models

In this study the standard k-ε model, the realizable k-ε, the standard k-ω, and the $\bar{v}^2 - f$ model were compared for simulating different cases of film cooling for flat plates. The Reynolds-averaged Navier-Stokes (RANS) equations were used as the transport equations for the mean flow. The governing equations and the detailed description of each model have been published elsewhere and therefore are not shown in this paper.

Standard k-ε model (SKE): The standard k-ε model is based on Launder and Spalding [7]. In this model, the Boussinesq assumption is applied together with wall functions.

Standard k-ω model (SKW): The standard k-ω model is a two equation model that solves for the transport of ω, the specific dissipation rate of the turbulent kinetic energy, instead of ε. It is based on that of Wilcox [8].

The $\bar{v}^2 - f$ model (V2F): According to Launder and Spalding [7], the normal stress $\bar{v}^2$ perpendicular to the local streamline plays the most important role to the eddy viscosity. Motivated by this idea, Durbin [9] devised a four-equation model, known as the k-ε-v^2 model or the $\bar{v}^2 - f$ model. It eliminates the need to patch models in order to predict wall phenomena like heat transfer or flow separation. It makes use of the standard k-ε model, but extends it by incorporating the anisotropy of near-wall turbulence and nonlocal pressure strain effects, while retaining a linear eddy viscosity assumption.

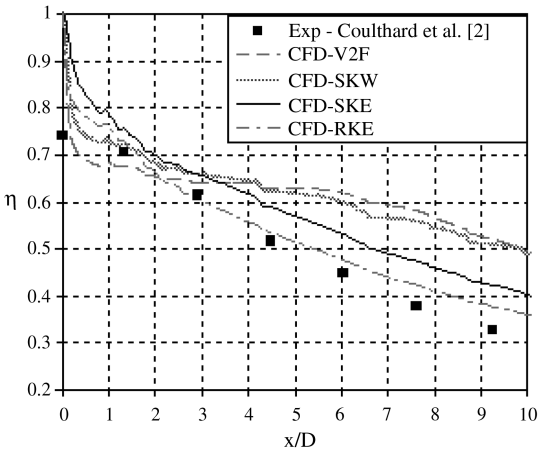

Fig. 2 Centerline plot of adiabatic effectiveness with different turbulence models compared with experimental data (CFH geometry, $B = 0.5$, steady blowing).

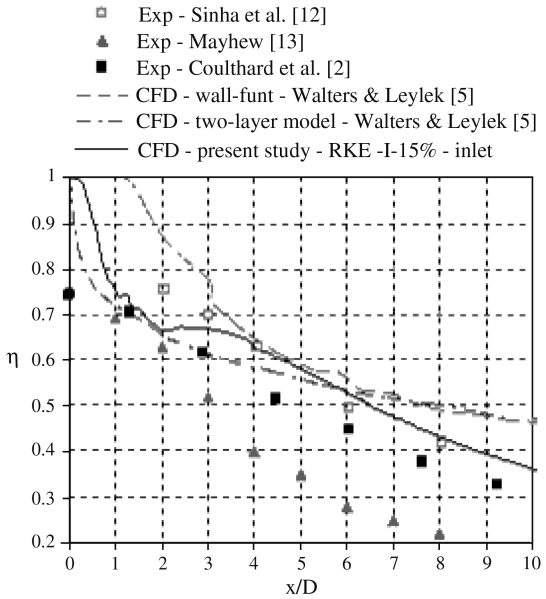

Fig. 3 Centerline adiabatic film-cooling effectiveness, $B - 0.5$, data from various experimental and computational studies compared with present work (CFH geometry).

Realizable k-ε model (RKE): A new k-ε eddy viscosity model proposed by Shih et al. [10] consists of a new model dissipation rate equation and a new realizable eddy viscosity formulation. The equation for the model dissipation rate is based on the dynamic equation of the mean-square vorticity fluctuation at large turbulent Reynolds number. In this model eddy viscosity formulation is based on the realizability constraints [under certain conditions (Shih et al. [10]), normal Reynolds stresses may become negative, which is unphysical (unrealizable)].

There is a common problem with RANS models when applied to jets in crossflow. This relates to the underprediction of the lateral spreading

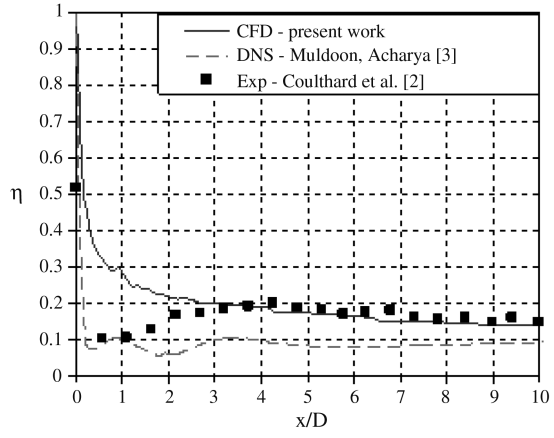

Fig. 4 Centerline adiabatic film-cooling effectiveness, steady state, $B = 1.5$ compared with DNS and experimental data (CFH geometry).

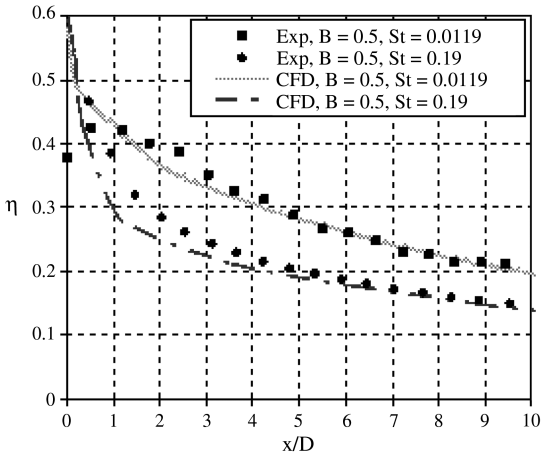

Fig. 5 Centerline plot of time-averaged adiabatic film-cooling effectiveness for $B = 0.5$, $St = 0.0119$, and $St = 0.19$ compared with experimental results (CFH geometry).

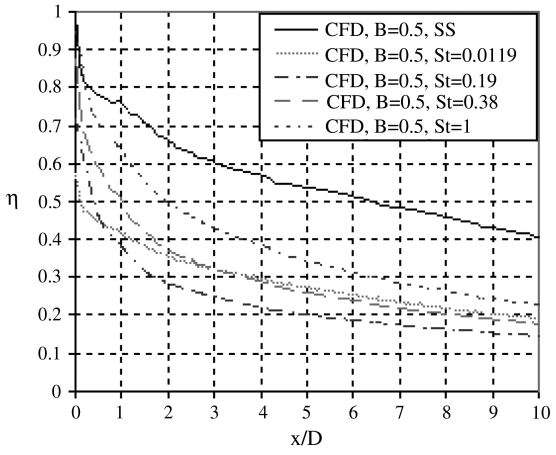

a)

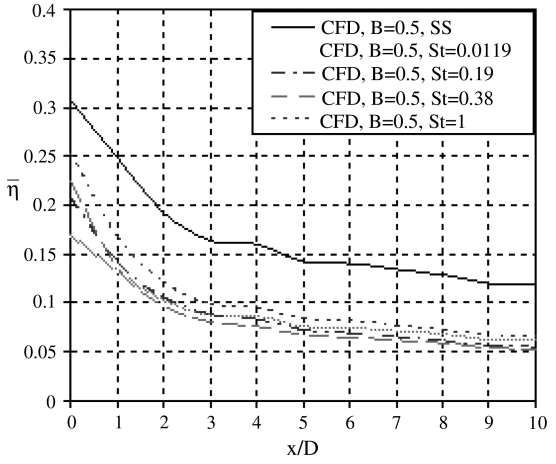

b)

Fig. 6 Centerline (a) and spanwise-averaged (b) plot of adiabatic film-cooling effectiveness for $B = 0.5$, steady state, and different Strouhal numbers.

and mixing of the jet (Acharya et al. [11]). However, using a higher level turbulence model (e.g., the Large-Eddy Simulation [LES]) would require more computational resources and limit the number of cases examined. Therefore, a decision was made to use RANS models for a comparative study and to provide qualitative trends.

IV. Results and Discussion

A. Code Validation

In this section the results obtained with different turbulence models are presented to validate the CFD model used to study pulsed jets film-cooling physics. Figure 2 shows results for centerline film-cooling effectiveness for the CFH geometry plotted versus x/D. Results were compared with the experimental data from Coulthard et al. [2]. Four different turbulence models were tested: V2F, RKE, SKW, and SKE. The inlet velocity profile used for the crossflow was obtained from the measured one (Coulthard et al. [2]) at $x/D = 0.8$ upstream of the jet. The SKE and RKE models showed the best overall performance. The SKW and V2F models were in a better agreement with the experimental data downstream of the jet-exit up to $x/D = 1.5$ and then showed over prediction compared with SKE and RKE models.

Based on the preceding results the RKE turbulence model was selected for further investigation for CFH geometry. Another reason for choosing RKE is that it resolves the problem that appears in the SKE turbulence model, when, under certain conditions (Shih et al. [10]), normal Reynolds stresses may become negative, which is unphysical (unrealizable).

At this step of the code validation our CFD results from the RKE model were compared against other CFD and experimental data. Figure 3 shows the centerline film-cooling effectiveness plotted versus x/D, $B = 0.5$ for different CFD and experimental data. The following was observed: 1) The variations in the film-cooling effectiveness among the experimentalists (Sinha et al. [12], Mayhew [13], and Coulthard et al. [2]) are due to differences in density ratio, injection-pipe length/diameter ratio, pitch-to-diameter ratio, crossflow inlet profile, and plenum geometry; 2) The CFD data from the present work (RKE turbulence model) are in good agreement with the experimental data from Coulthard et al. [2]. This is due to the fact that in this study the experimental setup (geometry, inlet flow conditions, etc.) was matched and the chosen RKE turbulence model performed well; 3) The other CFD data, from Walters and Leylek [5], shows the sensitivity of the CFD results to the geometry used as well as the turbulence model applied.

The effect of changing the blowing ratio from 0.5 to 1.5 under steady-state conditions was also examined in the present work. Coolant flow at the jet-exit is highly complex and depends on the blowing ratio. For $B = 0.5$ and CFH geometry, 61% of the mass flow were coming through the downstream half of the jet-exit plane. On the other hand, for $B = 1.5$, with the same geometry, about 49% of the mass flow were coming through the downstream half of the jet-exit plane. The reason behind that is the decrease in the effect of the

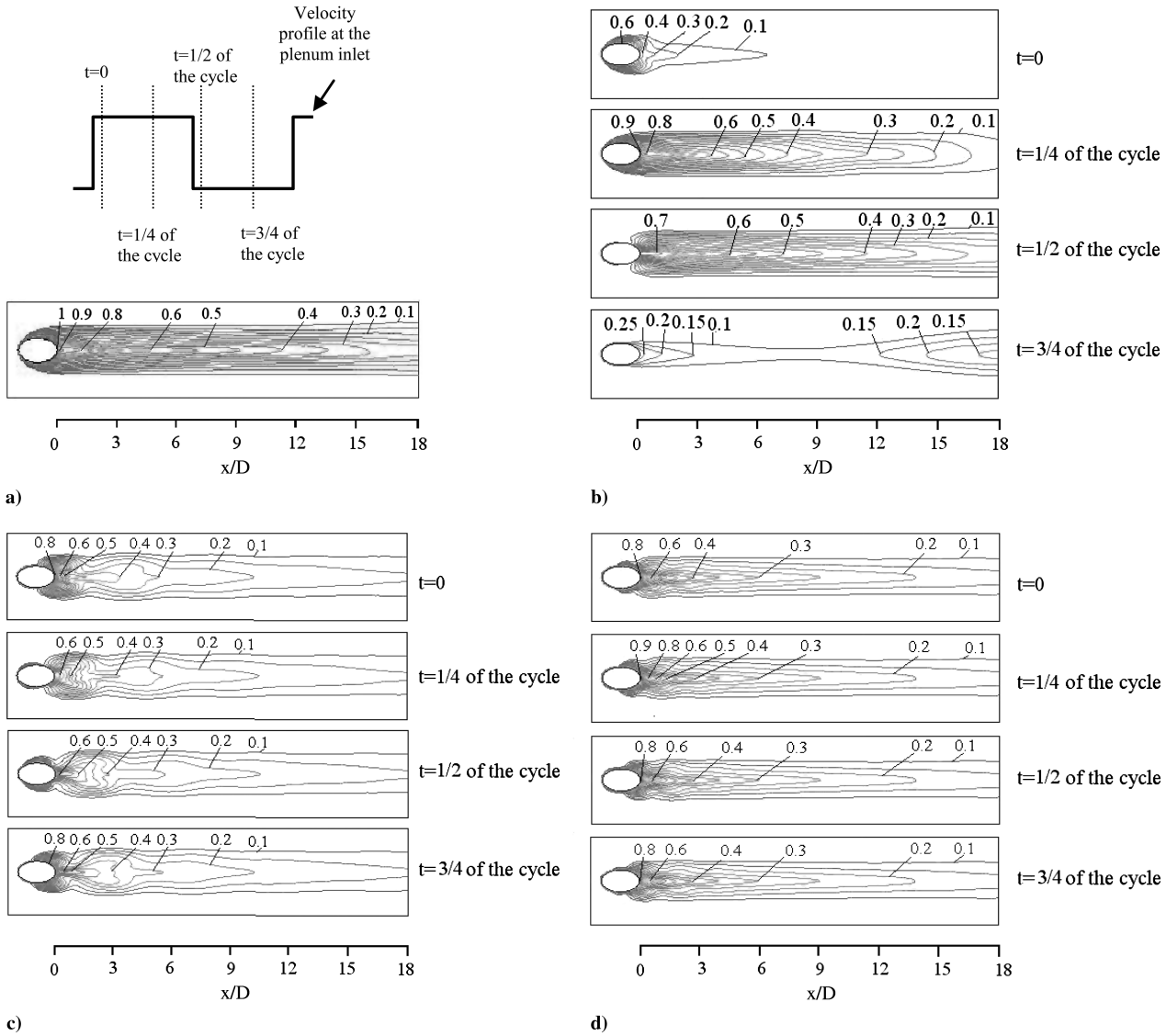

Fig. 7 Effectiveness footprints on the downstream wall, $B = 0.5$: a) steady state; b) $St = 0.0119$; c) $St = 0.19$; and d) $St = 0.38$ (CFH geometry).

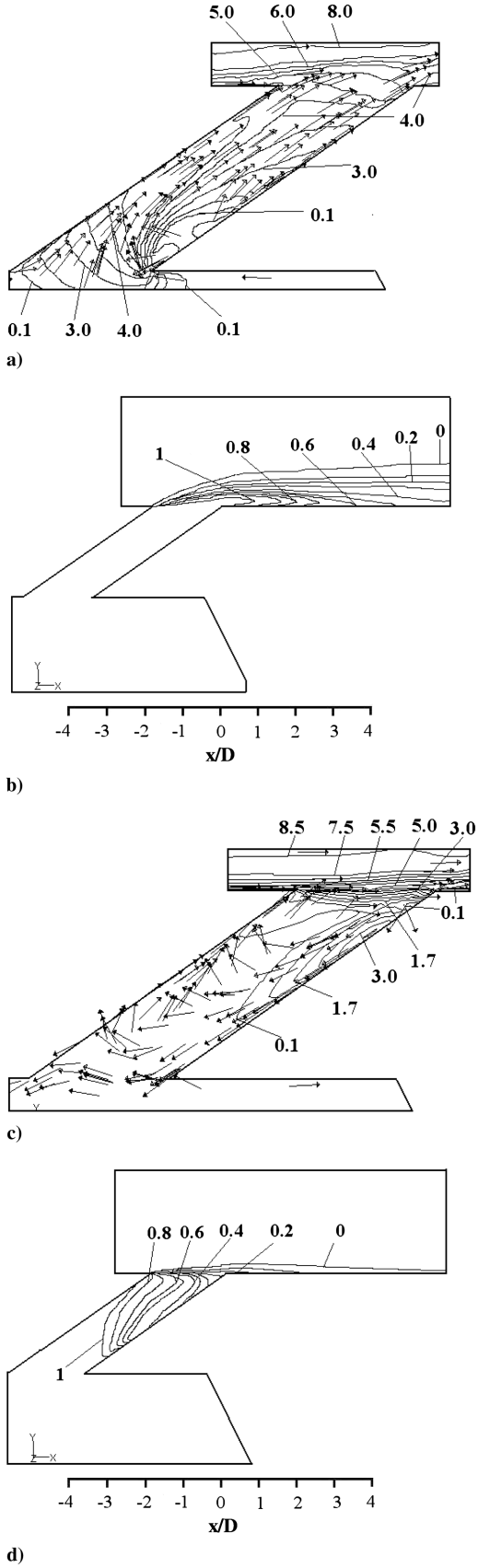

Fig. 8 CFH geometry, $B = 0.5$; velocity magnitude contours (m/s) and vectors: a) steady state; c) no blowing and dimensionless temperature side view; b) steady state; and d) no blowing.

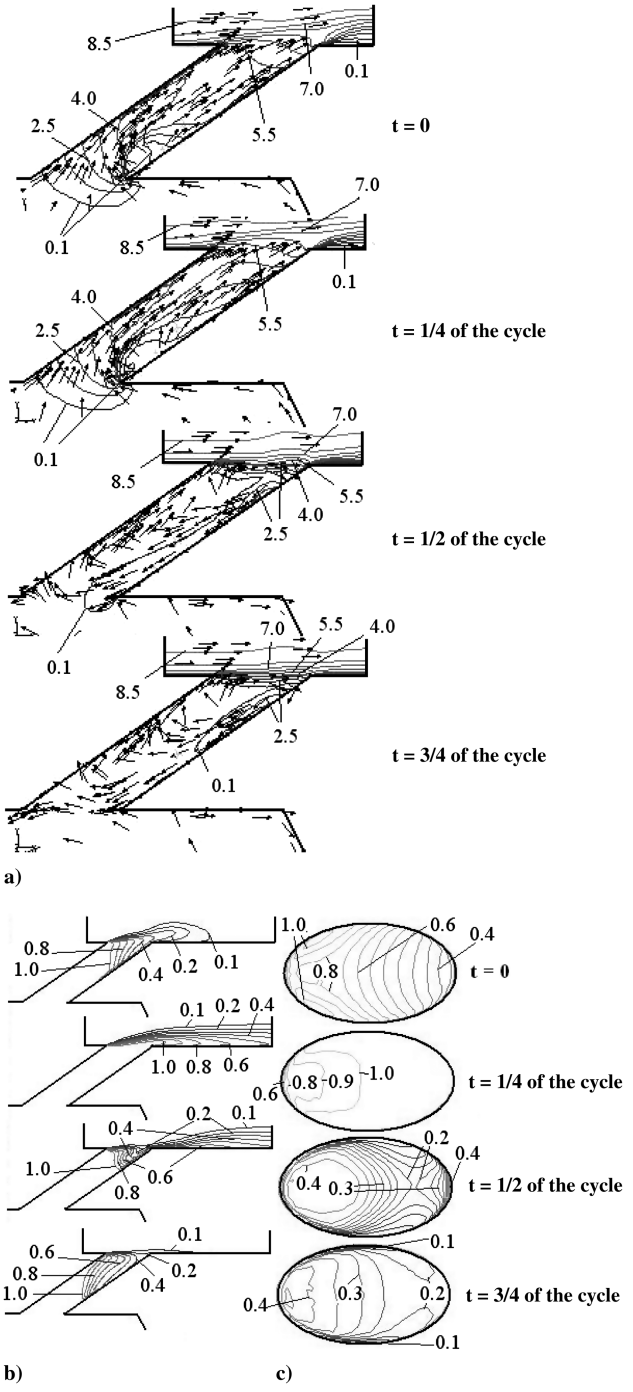

Fig. 9 $B = 0.5$, $St = 0.0119$: a) velocity magnitude contours (m/s) and vectors; b) dimensionless temperature side view; and c) dimensionless temperature contours at the jet top.

crossflow on the jet as coolant velocity increases. These data are consistent with Andreopoulos and Rodi [14].

Figure 4 shows comparison of the present CFD results (for centerline effectiveness) of the RKE model with DNS data from Muldoon and Acharya [3] and the experimental data of Coulthard et al. [2] for steady-state, $B = 1.5$ case. Our CFD model agreed very well with the experiment for $x/D > 2$, whereas the DNS data agreed better with the experimental data for $x/D < 2$.

Another step in the code validation was to compare current CFD model results with experimental data for the pulsed jets. Figure 5 shows results of the centerline film-cooling effectiveness versus x/D from Coulthard et al. [2] and the present model for $B = 0.5$ and pulsed jet with $St = 0.0119$ and $St = 0.19$. The CFD model showed overall good agreement with the data.

The current CFD results (not shown in this paper) for the spanwise film-cooling effectiveness showed underprediction (compared with experiments) similar to all RANS models attempted before. However, the effect of Strouhal number was negligible for the lateral jet spreading as reported by the experiment.

As can be seen from this section, the present CFD code with RKE turbulence model was validated by comparing its results with experimental and CFD data, including DNS, for both steady film-cooling flow and unsteady pulsed jets. This provided a confidence in this model such that it can be used to examine how the pulsed jet will be affected by 1) varying pulsation frequency and 2) blowing ratio. Each parameter will be discussed separately in the following sections.

B. Effect of Pulsation Frequency

The effect of pulsation frequency was examined for the CFH at different St. Figure 6a shows the centerline (time-averaged) film-cooling effectiveness for the CFH geometry with $B = 0.5$, steady state, $St = 0.0119$, 0.19, 0.38, and 1.0. The centerline film-cooling effectiveness, plotted versus x/D, showed that the effectiveness in the case of pulsation was always below the steady-state one. However, the effect of frequency varied according to the downstream location from the jet exit. Immediately near the jet trailing edge the effectiveness increased as the frequency increased. Downstream (x/D above three) the effectiveness for both $St = 0.0119$ and 0.38 were almost the same, whereas lower effectiveness was noted for $St = 0.19$. For $St = 1.0$ the effectiveness was the closest to steady-state case and for all x/D values. Figure 6b shows the spanwise-averaged film-cooling effectiveness plotted versus x/D for the same conditions of Fig. 6a. Similar results were obtained to those discussed in Fig. 6a, except the magnitude variations were much smaller. To examine these results further, (in Fig. 7) the effectiveness

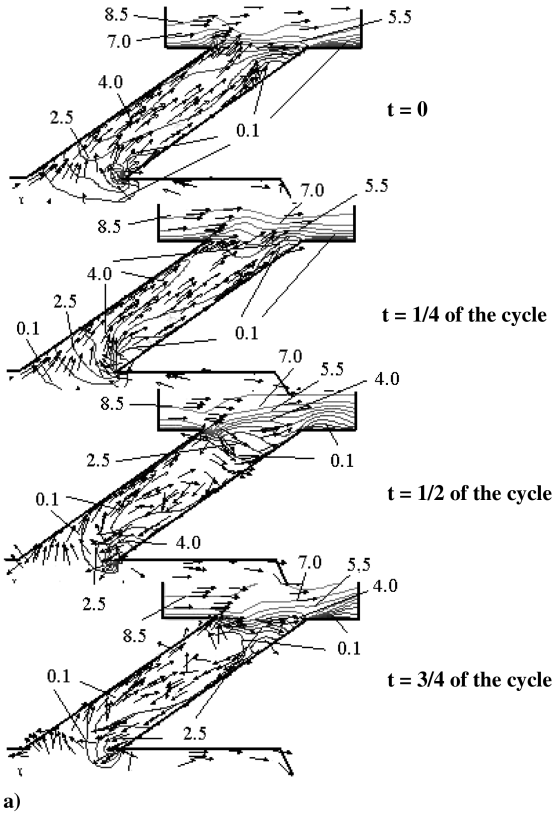

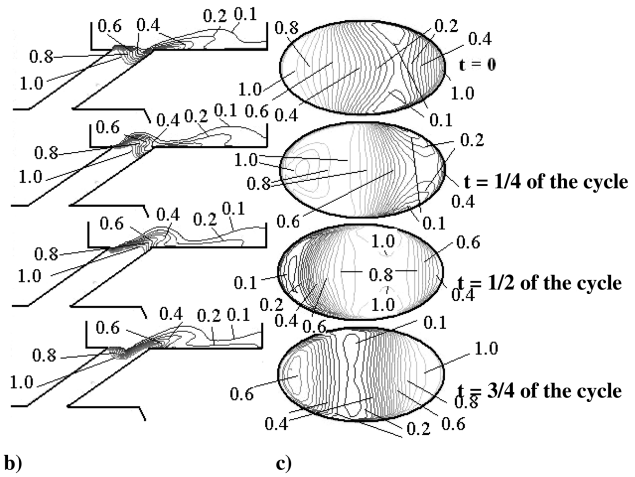

Fig. 10 $B = 0.5$, $St = 0.19$: a) velocity magnitude contours (m/s) and vectors; b) dimensionless temperature side view; and c) dimensionless temperature contours at the jet top.

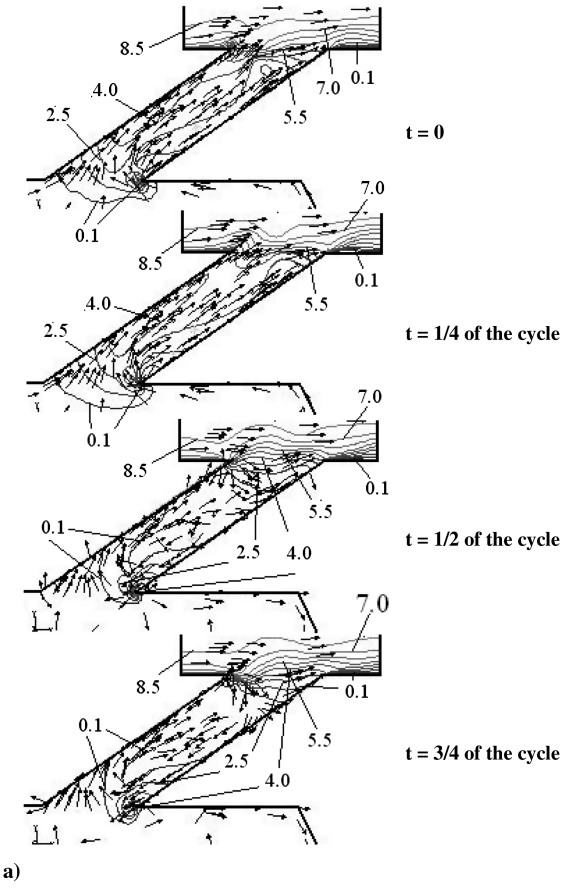

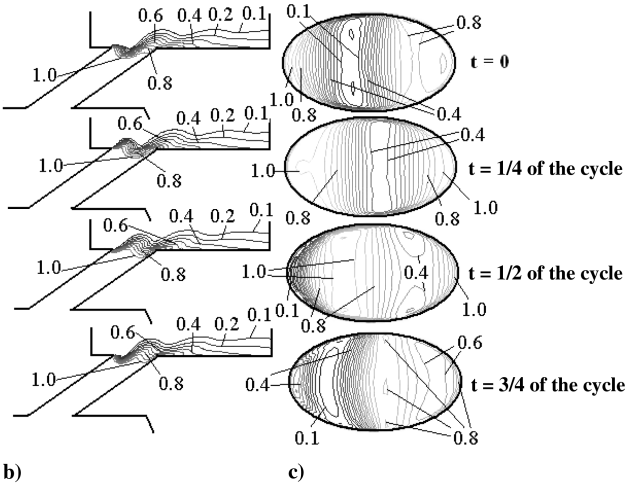

Fig. 11 $B = 0.5$, $St = 0.38$: a) velocity magnitude contours (m/s) and vectors; b) dimensionless temperature side view; and c) dimensionless temperature contours at the jet top.

footprints on the downstream wall were plotted for $B = 0.5$ as 7a steady state, 7b $St = 0.0119$, 7c $St = 0.19$, and 7d $St = 0.38$. The footprints are shown at different times in the cycle with DC = 50%, at $t = 0$ (the beginning of blowing), $t = \frac{1}{4}$ (middle of blowing), $t = \frac{1}{2}$ (end of blowing), and finally $t = \frac{3}{4}$ (middle of no blowing). Figure 7a shows the steady-state results with high effectiveness downstream of the jet. Figure 7b shows the results of $St = 0.0119$ where we see high effectives, similar to the steady-state one, only on a small window of the cycle (near $t = 1/4$ and $t = 1/2$, only downstream of the jet) indicating a quasi-steady behavior. Otherwise (i.e., at other times of the cycle), the jet film-cooling effectiveness is very poor. As the frequency increased (Fig. 7c) the footprints of the film-cooling effectiveness took a more complicated shape, showing considerable variation in the spanwise direction at different times of the cycle, with a net effect of lower effectiveness throughout the cycle and the lowest (time-averaged values) at $St = 0.19$ (as shown earlier in Fig. 6a). Figure 7d is for the higher frequency ($St = 0.38$) and shows a return to the quasi-steady behavior shown at lower frequencies ($St =$ 0.0119). This, of course, will result in a higher time-averaged film-cooling effectiveness as shown earlier but still below the steady-state one. Similar observations were noted for $St = 1.0$ (not shown in this paper) to what was discussed at $St = 0.38$.

To understand the behavior described previously, movies were generated for the side-view temperature contours at the center plane (corresponds directly to the film-cooling effectiveness for an adiabatic wall) for different Strouhal numbers. This was done for the following cases: 1) steady-state conditions, 2) shut down of the film-cooling injection from the plenum inlet (this will correspond to a very low-frequency case just before the blowing starts), 3) $St = 0.0119$, 4) $St = 0.19$, and e) $St = 0.38$. These cases will be discussed in the following section.

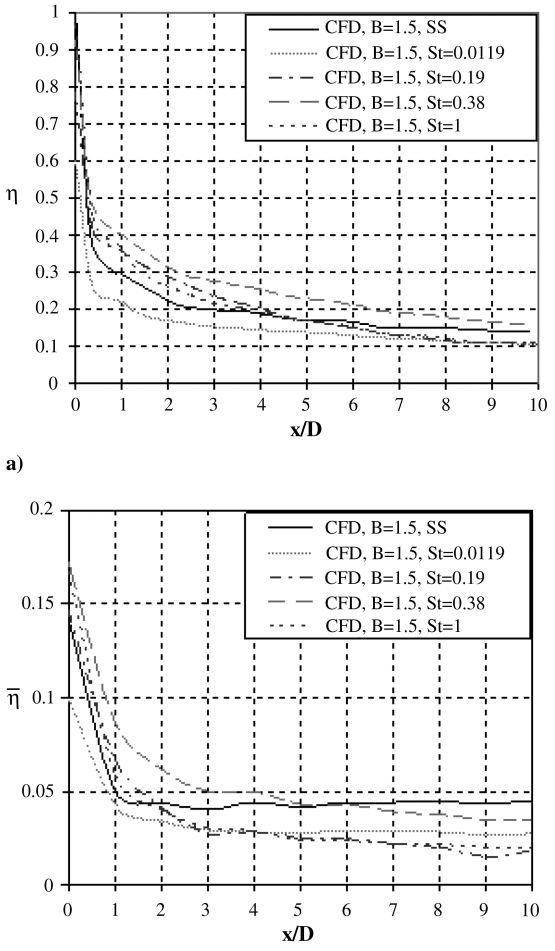

Fig. 12 Adiabatic film-cooling effectiveness for $B = 1.5$ steady state and different Strouhal numbers: a) centerline and b) spanwise averaged.

Figure 8a shows the velocity contours and vectors for the steady-state $B = 0.5$ case, CFH geometry. It can be seen that because of the inclusion of the plenum geometry in the computation domain, a nonuniform flow entered the injection pipe with a recirculation taking place near the forward bottom side of the pipe. This, in turn, resulted in highly nonuniform flow at the jet outlet (a local velocity up to 5 m/s, 25% higher than the nominal blowing velocity for $B = 0.5$). Figure 8b shows a side view of the dimensionless temperature contours for the same case. The cold fluid was filling the whole injection pipe and a good coverage was provided downstream the jet. The flow from the plenum inlet was then shut off and the CFD case was run until it reached final steady-state conditions. Figure 8c shows the velocity contours and vectors in the injection pipe. Velocity of about 3 m/s (in the crossflow direction) was noticed at the jet-exit plane. Recirculation zone, similar to the cavity-driven flow, existed in the injection pipe. Figure 8d shows the temperature contours where the hot fluid penetrates into the injection pipe almost up to the plenum exit plane. This observation is significant, as will be seen in the following section discussing the pulsed jet.

Figures 9a, 10b, and 11a show the velocity contours and vectors in the injection pipe for $St = 0.0119$, 0.19 and 0.38, respectively, at four different times of the cycle ($t = 0, \frac{1}{4}, \frac{1}{2}, \frac{3}{4}$). Side view of the dimensionless temperature contours for the same cases are shown in Fig. 9b ($St = 0.0119$), Fig. 10c ($St = 0.19$), and Fig. 11b ($St =$ 0.38). Also, dimensionless temperature contours (top view of the jet) for the same cases are shown in Fig. 9c ($St = 0.0119$), Fig. 10d ($St = 0.19$), and Fig. 11c ($St = 0.38$).

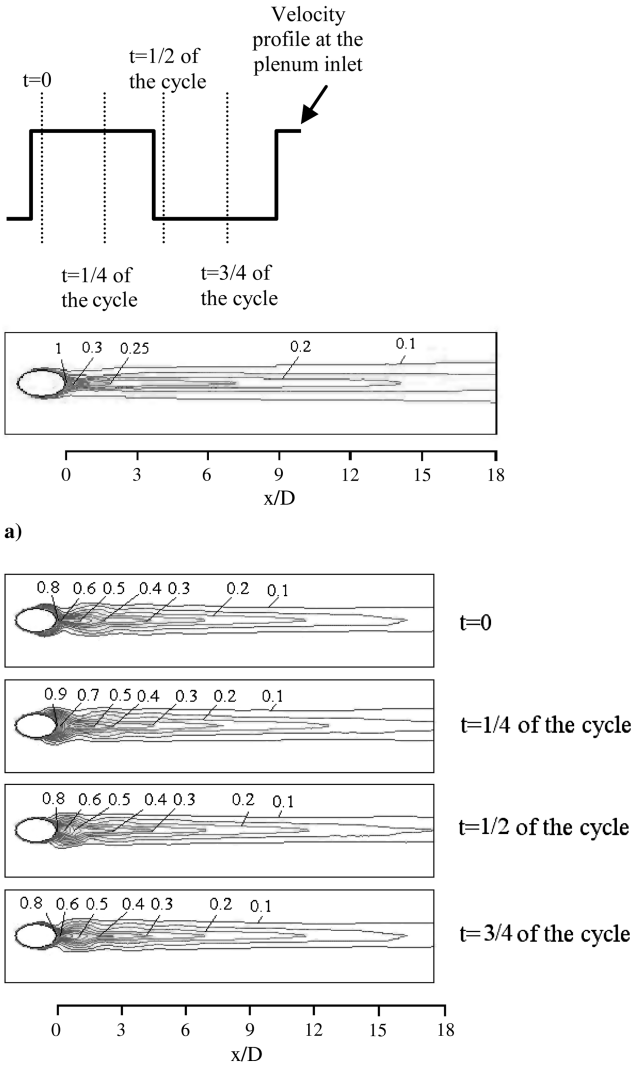

Fig. 13 Effectiveness footprints on the downstream wall, $B = 1.5$: a) steady state and b) $St = 0.38$.

For the case of $St = 0.0119$ (Fig. 9) and at $t = 0$, a bubble of hot fluid was seen in the temperature-contour side view, which was the remainder from the previous cycle. Notice this appeared only at the lowest Strouhal number studied. The outcome was the low dimensionless temperature at the jet-exit plane as shown in Fig. 9c. At $t = \frac{1}{4}$ the jet reached a full blown level and appeared very similar to the steady-state condition (Figs. 8a and 8b) and accordingly, the best film-cooling effectiveness occurred. At $t = \frac{1}{2}$ the flow started to retard in the injection pipe, allowing more flow from the cross stream to get into the pipe. The cooling effectiveness of the jet decreased as shown at the jet-exit plane (Fig. 9c). Finally at $t = \frac{3}{4}$ the flow penetrated further into the injection pipe allowing a hot bubble to enlarge and reach to more than half of the injection pipe. Accordingly, very low film-cooling effectiveness was obtained.

For the case of $St = 0.19$ (Fig. 10) and at $t = 0$, a smaller (than the previous case with $St = 0.0119$) bubble was seen from the velocity vectors and the temperature-contour side view as a result of the higher frequency (lower cycle time). Thus, there was not enough time to form a larger sized bubble that would be ingested inside the injection pipe (as shown earlier at $St = 0.0119$). At $t = \frac{1}{4}$ the jet did not reach a full-blown level (due to lesser cycle time) and thus, less film-cooling effectiveness at the jet-exit plane occurred (compare Fig. 10d with Fig. 9c at $t = \frac{1}{4}$). At $t = \frac{1}{2}$ the flow started to retard in the injection pipe but would not allow more flow from the cross stream to get into the pipe (again due to lesser cycle time). The cooling effectiveness of the jet decreased as shown at the jet-exit plane (Fig. 10d). Finally at $t = \frac{3}{4}$ the flow penetrated further into the injection pipe allowing a hot bubble to exist in the injection pipe. Accordingly, lower film-cooling effectiveness was obtained.

For the case of $St = 0.38$ (Fig. 11) and at $t = 0$, no bubble was seen from the velocity vectors and the temperature-contour side view as a result of the high frequency (low cycle time) and thus, there was not enough time to form that bubble inside the injection pipe (as shown earlier at $St = 0.0119$). At $t = \frac{1}{4}$ the jet did not reach a full-blown level (due to lesser cycle time) and thus, less film-cooling effectiveness at the jet-exit plane (compare Fig. 11c with Fig. 10d at $t = 1/4$). At $t = \frac{1}{2}$ the flow started to penetrate into the injection pipe but would allow even less flow from the cross stream to get into the pipe (compare Figs. 11b and 11c with Figs. 10c and 10d at $t = \frac{1}{2}$). This was, again, due to lesser cycle time. The cooling effectiveness of the jet stayed almost the same as shown at the jet exit.

From the different frequencies just examined, two opposing factors were noticed: 1) low frequency (high-cycle time) will allow more time (during blowing) for full-blown jet flow and thus high film-cooling effectiveness and 2) this high-cycle time, however, will provide more time during jet shutoff and thus more time for the crossflow to penetrate and be ingested into the injection pipe. This will create low effectiveness during shutoff and the beginning of the

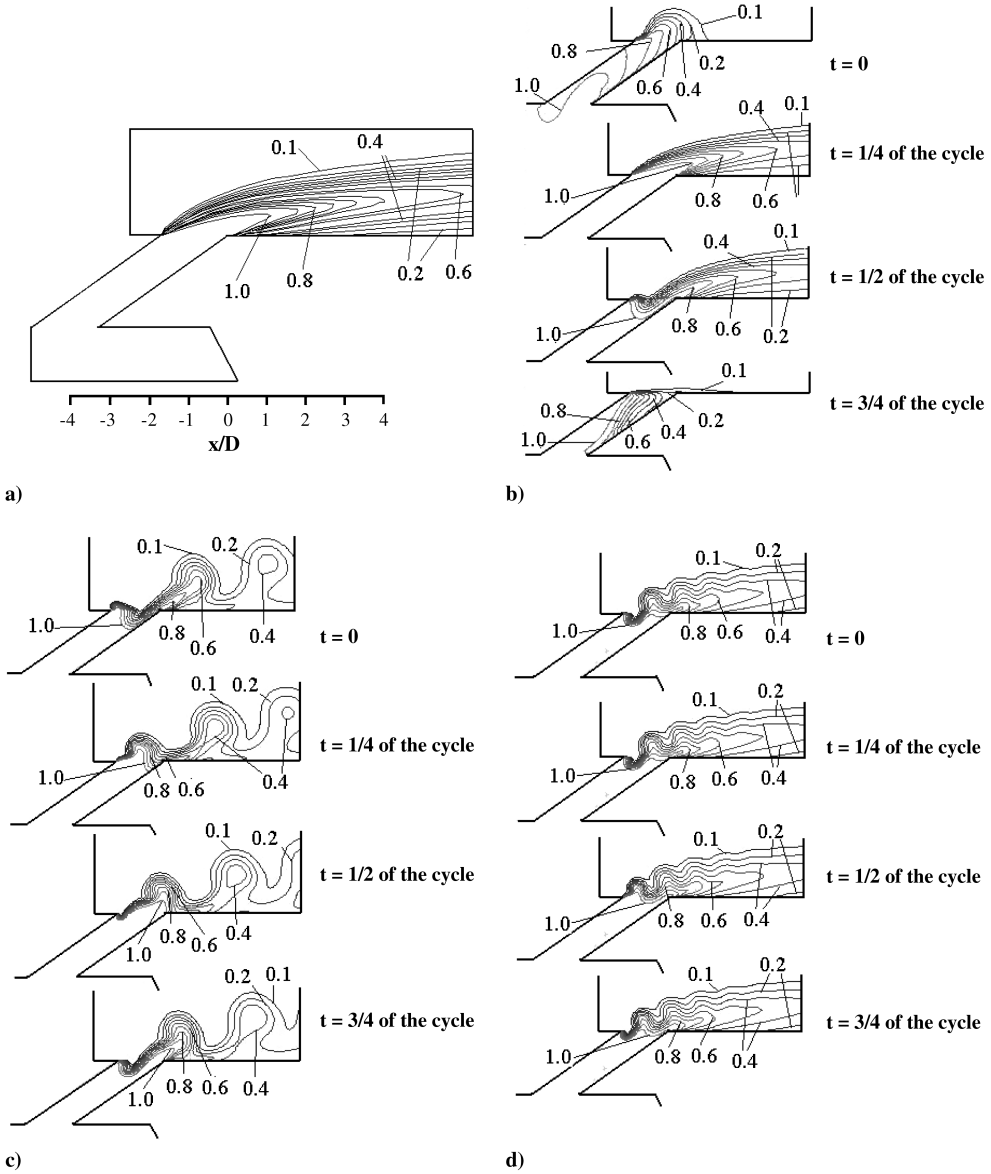

Fig. 14 Dimensionless temperature side view, $B = 1.5$: a) steady state; b) $St = 0.0119$; c) $St = 0.38$; and d) $St = 1$.

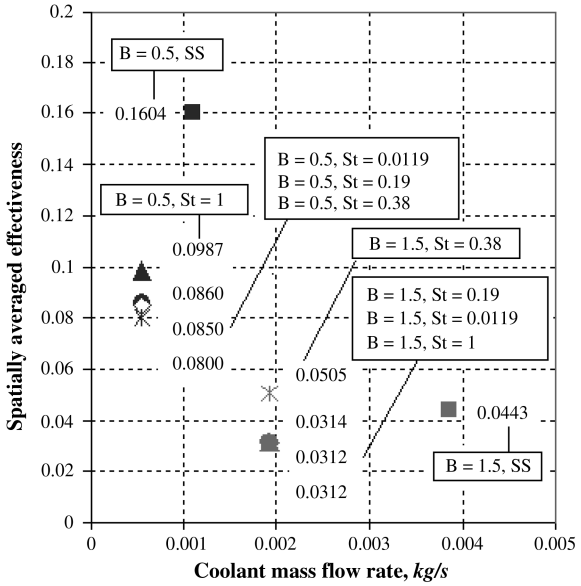

Fig. 15 Film-cooling characteristics, averaged over $x/D = 10$ by $z/D = 3$ area, for all studied cases.

blowing time. The net effect of these two factors is what was shown earlier in Fig. 6. It should be noted that those observations are geometry-dependent as they apply only to CFH geometry.

C. Effect of Jet Blowing Ratio

Two different blowing ratios were examined as was described earlier, for the CFH, steady state, $St = 0.0119$, 0.19, 0.38, and 1.0. Figure 12a shows the centerline (time-averaged) film-cooling effectiveness for the CFH geometry with $B = 1.5$ (to be compared with Fig. 6a for $B = 0.5$). Figure 12b shows the spanwise-averaged (and time-averaged) effectiveness under similar conditions. Because the effect of pulsation was very small in the spanwise compared with the centerline effectiveness, our focus will be on the results shown in Fig. 12a. First, as expected, for steady state as the blowing ratio changed from 0.5 to 1.5 the film-cooling effectiveness became much lower everywhere due to the jet liftoff at the higher B values. The pulsation had different effects in the two cases. At $B = 0.5$ (as discussed earlier) lower effectiveness performance was obtained everywhere, compared with the steady state. For $B = 1.5$ pulsation results were highly dependent on the frequency. For low frequency ($St = 0.0119$) the effectiveness was below the steady-state values for all x/D values. For higher frequency ($St = 0.38$) the effectiveness was higher than the steady-state values for all x/D locations. As for $St = 0.19$ and 1.0 the results were in between these two frequencies. To understand this behavior better, Figs. 13 and 14 were shown.

Figure 13 shows the effectiveness footprints on the downstream wall, $B = 1.5$, for: 13a steady state, and 13b $St = 0.38$. The footprints are shown at different time in the pulsation cycle with 50% duty cycle, at four different times of the cycle ($t = 0, \frac{1}{4}, \frac{1}{2}, \frac{3}{4}$). Figure 13a shows the steady state with low effectiveness downstream of the jet. Figure 13b shows the results of $St = 0.38$ where the effectives were higher than the steady state at all times of the cycle. This, of course, will result in a higher time-averaged film-cooling effectiveness (at all x/D) as shown in Fig. 12a and above the steady-state one.

Figure 14a shows the dimensionless temperature contours (side view), for steady state. At four different times of the cycle ($t = 0, \frac{1}{4}, \frac{1}{2}, \frac{3}{4}$), the dimensionless temperature contours (side view) are shown for $St = 0.0119$ (Fig. 14b), $St = 0.38$ (Fig. 14c), and $St = 1.0$ (Fig. 14d). Figure 14a shows the jet liftoff that results in a low film-cooling effectiveness. Figure 14b ($St = 0.0119$) shows how the high cycle time (low frequency) allows two mechanisms to happen: 1) jet liftoff to exist (while jet is open) and 2) cross-stream flow to be ingested into the injection pipe (while jet is closed). Both factors were affecting the effectiveness negatively and resulted in lower values at all x/D value (compared with steady state). Figure 14c ($St = 0.38$) shows how the jet breaks up due to both the jet liftoff and pulsation, which provides a continuous supply of coolant on the top surface and thus, higher effectiveness at all x/D value (compared with steady state). Figure 14d ($St = 1.0$) shows that the jet liftoff does exist throughout the duration of the cycle and only the upper part of the jet (which interacts with the cross stream) is affected by the pulsation. This in turn resulted in lower centerline effectiveness compared with the case with $St = 0.38$ but slightly higher than the steady-state one.

D. Spatially Averaged Film-Cooling Effectiveness

The film-cooling effectiveness examined in this paper varied spatially and temporally. Spatially averaged effectiveness was used to compare overall performance of all cases examined. We chose an area downstream the jet that covered from the jet trailing edge, $x/D = 0$ to $x/D = 10$ and also covered a $\frac{1}{2}$ pitch on both sides of the jet in the spanwise direction. It is clear that the area choice might alter the results of this section. Then we averaged the film-cooling effectiveness over this area spatially and then temporally. Figure 15 shows this spatially averaged effectiveness plotted versus the coolant mass flow rate (kg/s) for all cases examined in this paper. Table 2 summarizes the results.

As noted earlier, the duty cycle in the present study was kept constant at 50%. Table 2 shows that using the defined spatially averaged effectiveness and using 50% of the coolant will result in the following: 1) an overall reduction of 38.12% for $B = 0.5$ and 2) an overall enhancement of 14.77% for $B = 1.5$. Those results indicate that jet pulsation is more effective for cases with detached jets (e.g., CFH geometry and $B = 1.5$) under steady-state conditions.

Pulsed jets performance significantly depends on pulsation frequency and blowing ratio. Another important factor (which was observed but not discussed in this paper) is the pulsed jet attenuation due to the plenum geometry. While a square flow wave was applied at the plenum inlet, the flow that comes out of the jet depends on plenum geometry, jet geometry, pulsation frequency, and blowing ratio, among others.

Pulsation helps to lower the amount of cool air from the compressor, which is desirable for film-cooling applications. However, for the conditions in which steady blowing performs well, pulsation considerably decreases the film-cooling effectiveness. For the cases where steady blowing gives poor results due to the detached jet (higher blowing ratios), pulsation helps to increase time and distance-averaged effectiveness (provides reduction in jet liftoff) when coolant amount decreases. Although pulsation does not bring overall benefit to film cooling, there are cases where pulsed jets help to increase effectiveness over steady-state case. Therefore, present results might be used to evaluate the effect of pulse frequency on film-cooling effectiveness in real life applications, where jets pulse naturally due to the pressure fluctuations in the engine.

V. Conclusions

The effect of pulsation frequency on flat plate film-cooling effectiveness was examined for CFH geometry, $B = 0.5$ and 1.5,

Table 2 Spatially averaged effectiveness ($\bar{\bar{\eta}}$) for all cases examined in this paper

Geometry	Blowing ratio	$\bar{\bar{\eta}}$ for steady state	$\bar{\bar{\eta}}$ (highest value) for pulsed jet	$\bar{\bar{\eta}}$ % change (pulsed/steady state − 1)*100
CFH	0.5	0.16	0.099	−38.12
CFH	1.5	0.044	0.0505	14.77

$St = 0.0119$, 0.19, 0.38, and 1.0. Because the effect of pulsation was very small in the spanwise compared with the centerline effectiveness, the focus of this study was on results for the centerline effectiveness.

For $B = 0.5$ and all frequencies examined, the CFD results showed that the pulsed jet has lower film-cooling effectiveness than the steady state. These results are attributed to the fact that jet flow provided good surface coverage during the blowing period, whereas during the shutoff time there was a chance of the hot crossflow to be ingested into the injection pipe.

For $B = 1.5$ pulsation results were highly dependent on the frequency. At low frequency (e.g., $St = 0.0119$) the effectiveness was below the steady state for all x/D values. These results are attributed to the fact that jet flow provided poor surface coverage (due to jet liftoff) during the blowing period, whereas during the shutoff time there was a chance of the hot crossflow to be ingested into the injection pipe. Both factors were affecting the effectiveness negatively and resulted in lower values at all downstream x/D locations. For higher frequency (e.g., $St = 0.38$), however, the effectiveness was higher than the steady-state values for all downstream x/D locations. In this case the jet broke up due to both the jet liftoff and pulsation, which provided a continuous supply of coolant on the top surface and thus higher effectiveness at all x/D value. As for $St = 0.19$ and 1.0 the results were in between the two frequencies just discussed. For $St = 1.0$ the jet liftoff did exist throughout the duration of the cycle and only the upper part of the jet (which interacts with the cross stream) was affected by the pulsation. This in turn resulted in lower centerline effectiveness compared with the case with $St = 0.38$ but slightly higher than the steady-state one.

A spatially averaged effectiveness ($\bar{\bar{\eta}}$) was computed to compare overall performance of all cases examined. Using the defined $\bar{\bar{\eta}}$ with 50% of the coolant (under $DC = 50\%$) the best results (of all cases examined) was found to be 1) an overall reduction of 38.12% for $B = 0.5$ and 2) an overall enhancement of 14.77% for $B = 1.5$.

Pulsed jets performance significantly depends on geometry and blowing ratio. Pulsation helps to lower the amount of cool air from the compressor, which is desirable for film-cooling applications. However, for the conditions of steady blowing and attached jet, pulsation considerably decreases the film-cooling effectiveness. For the cases of steady blowing and jet liftoff (e.g., higher blowing ratios), pulsation helps to increase time and distance-averaged effectiveness when coolant amount decreases. Although pulsation did not bring overall benefit to film cooling, there are cases where pulsed jets help to increase effectiveness over steady-state case.

Acknowledgments

This work was performed under partial sponsorship from the U.S. Department of Energy with Michael Knaggs as contract monitor. Department of Energy grant number DE-FC26-06NT42853. The first author gratefully acknowledges support from Zonta International Amelia Earhart Fellowship.

References

[1] Ekkad, S. V., Ou, S., and Rivir, R. B., "Effect of Jet Pulsation and Duty Cycle on Film Cooling from a Single Jet on a Leading Edge Model," *ASME Journal of Turbomachinery*, Vol. 128, No. 3, 2006, pp. 564–571. doi:10.1115/1.2185122

[2] Coulthard, S. M., Volino, R. J., and Flack, K. A., "Effect of Jet Pulsing on Film Cooling, Part 1: Effectiveness and Flowfield Temperature Results," *ASME Journal of Turbomachinery*, Vol. 129, No. 2, 2007, pp. 232–246. doi:10.1115/1.2437231

[3] Muldoon, F., and Acharya, S., "Computation of Pulsed Film Cooling," American Society of Mechanical Engineers Paper GT2007-28156, 2007.

[4] FLUENT, Inc., Fluent 6.3: User's Guide, 2005.

[5] Walters, D. K., and Leylek, J. H., "A Systematic Computational Methodology Applied to a Three-Dimensional Film-Cooling Flowfield," *ASME Journal of Turbomachinery*, Vol. 119, No. 4, 1997, pp. 777–785.

[6] Walters, D. K., and Leylek, J. H., "A Detailed Analysis of Film-Cooling Physics: Part 1—Streamwise Injection with Cylindrical Holes," *ASME Journal of Turbomachinery*, Vol. 122, No. 1, 2000, pp. 102–112. doi:10.1115/1.555433

[7] Launder, B. E., and Spalding, D. B., "The Numerical Computation of Turbulent Flows," *Computer Methods in Applied Mechanics and Engineering*, Vol. 3, No. 2, 1974, pp. 269–289. doi:10.1016/0045-7825(74)90029-2

[8] Wilcox, D. C., *Turbulent Modeling for CFD*, DCW Industries, Inc., La Canada, California, 1998.

[9] Durbin, P. A., "Separated Flow Computations with the k-ε-v^2 Model," *AIAA Journal*, Vol. 33, No. 4, 1995, pp. 659–664. doi:10.2514/3.12628

[10] Shih, T. H., Liou, W. W., Shabbir, A., Yang, Z., and Zhu, J., "A New k-ε Eddy Viscosity Model for High Reynolds Number Turbulent Flows," *Computers Fluids*, Vol. 24, No. 3, 1995, pp. 227–238. doi:10.1016/0045-7930(94)00032-T

[11] Acharya, S., Tyagi, M., and Honda, A., "Flow and Heat Transfer for Film Cooling," *In Heat Transfer in Gas Turbine Systems*, Vol. 934, Annals of the New York Academy of Sciences, New York, New York, 2001, pp. 110–125.

[12] Sinha, A. K., Bogard, D. G., and Crafword, M. E., "Film Cooling Effectiveness Downstream of a Single Row of Holes with Variable Ratio," *ASME Journal of Turbomachinery*, Vol. 113, No. 3, 1991, pp. 442–449. doi:10.1115/1.2927894

[13] Mayhew, J. E., "An Experimental Investigation of the Effect of Freestream Turbulence on Film Cooling Using Thermochromic Liquid Crystal Thermography," Ph.D., Dissertation, University of California, Davis, CA, 1999.

[14] Andreopoulos, J., and Rodi, W., "Experimental Investigation of Jets in a Crossflow," *Journal of Fluid Mechanics*, Vol. 138, No. 1, 1984, pp. 93–127. doi:10.1017/S0022112084000057

F. Liu
Associate Editor